On Energy Harvesting Module for Scalable Cognitive Autonomous Nondestructive Sensing Network ($SCANS^n$) System for Bridge Health Monitoring

John Turner[1], Justin Cartwright[1], Dong Sam Ha[1], David Zhang[2], Sourav Banerjee[2]
[1]Center for Embedded Systems for Critical Applications (CESCA)
Bradley Department of Electrical and Computer Engineering, Virginia Tech, Blacksburg, VA 24061
[2]Acellent Technologies Inc. 835 Stewart Drive, CA 84085

ABSTRACT

The $SCANS^n$ is a structural health monitoring (SHM) system is being developed by Acellent Technologies to monitor steel bridges. The required voltage of the system is 14.4 V for active scanning, and the power consumption is approximately 8 W. The investigated energy harvesting from both solar and thermal sources to recharge the lithium-ion battery of the system. A solar panel and a Thermal Electric Generator (TEG) are used to harvest ambient energy. The thermoelectric device is placed in a Fresnel dome to maximize the temperature gradient of the TEG. During shading of the solar panel, the TEG continues to supply power to the battery charger. Since the output voltages and currents of the solar and thermal energy harvesters vary significantly, the energy harvesting module is constructed by two buck-boost converters operating in parallel. Maximal Power Point Tracking (MPPT) is employed for the buck-boost converter for the solar panel, while a fixed duty cycle converter is used for the TEG due to substantially lower power compared with the solar panel. The system design and measured results of a prototype system are presented. Our prototype system successfully demonstrates that the $SCANS^n$ system can be powered by the energy harvested from solar and thermal.

Keywords: energy harvesting, solar, thermal electric generator, battery charging, SHM

1. INTRODUCTION

Structural Health Monitoring (SHM) is the science and technology of monitoring and assessing the condition of aerospace, civil, and mechanical infrastructures using a sensing system integrated into the structure. SHM is capable of detecting, locating, and quantifying various types of damage such as cracks, holes, corrosion, delamination, and loose joints, and can be applied to various infrastructures such as buildings, railroads, windmills, bridges, and aircrafts.

Acellent Technologies has developed a SHM system named $SCANS^n$ (Scalable Cognitive Autonomous Nondestructive Sensing Network) for deployment on bridges. The $SCANS^n$ system consumes 4.88 W-hours within a 24-hour period and dissipates 8 W during active scanning, and the system is currently powered by a 14.4 V rechargeable battery. However, this requirement will be dramatically reduced in next generation development using ASIC design. Recharging or replacing batteries for the $SCANS^n$ system would be expensive, since line power may not be available on bridges and laying out of cables is undesirable or costly. To address the problem, it was proposed that the system could be powered with energy harvested from ambient sources, specifically solar and thermal. A solar panel and a Thermal Electric Generator (TEG) are used to harvest ambient energy. During shading of the solar panel, the TEG continues to supply power to the battery charger. Since the output voltages and currents of the solar and thermal energy harvesters vary significantly, the energy harvesting module is constructed by two buck-boost converters operating in parallel. A low power microcontroller performs Maximum Power Point Tracking (MPPT) for the solar panel, while a fixed duty cycle converter is used for the TEG.

The paper is organized in the following manner. Section 2 presents characteristics of solar panels and TEGs, a commonly used scheme for lithium-ion battery charging, and the basic operation of a buck-boost converter. Section 3 covers system overview, circuit design, and the MPPT algorithm employed for the proposed system. Section 4 presents experimental results of our prototype in progress, and Section 5 summarizes the paper.

Nondestructive Characterization for Composite Materials, Aerospace Engineering, Civil Infrastructure, and Homeland Security 2011, edited by H. Felix Wu, Proc. of SPIE Vol. 7983, 79831T · © 2011 SPIE
CCC code: 0277-786X/11/$18 · doi: 10.1117/12.880286

2. PRELIMINARIES

In this section, preliminaries are provided about solar panels, TEGs, battery chargers, and buck-boost converters related to or adopted for our system.

2.1 Solar Panel and TEG Output Characteristics

The output of a solar panel is a function of solar irradiance, air mass, and temperature. Figure 1 shows an example I-V for a generic solar panel. The panel acts as a current source at low terminal voltages, exhibiting a high output resistance. The red circle of an I-V curve indicates maximum power point (MPP), where maximum power is transferred from the panel. The panel acts more like a voltage source beyond the MPP point. The open circuit voltage and short circuit current increase as the solar irradiance increases as shown in the figure. An important issue is that the MPP changes as the solar irradiance (as well as other operating conditions such as the temperature) changes. The load resistance, therefore, should change dynamically to transfer the maximum power from the panel to the load.

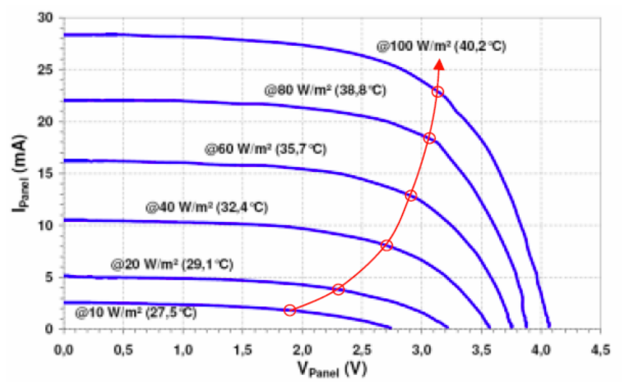

Figure 1.I-V Characteristics of a Generic Solar Panel [1]

A TEG consists of semiconductor material located between two plates, a hot surface and a cool one. The output characteristics of a TEG depend on both the temperature gradient across the device and the average temperature of the TEG's plates. The output characteristics of an example TEG for a given hot and cool side temperatures are shown in Figure 2. The load resistance of the device is varied from 0 - 20 Ω. The output voltage and current are shown in red and green respectively while the output power is plotted in blue. Like a solar panel, the maximum power transfer occurs for an optimal load resistance, and that optimal resistance changes as the temperature gradient and/or absolute temperature varies. Thus, it requires dynamic change of the load resistance for a maximum power transfer from a TEG.

Our SCANS^n system targets for structural health monitoring of bridges. Hence, the temperature gradient for our TEGs would be small to harvest only a small amount of energy. So that the benefit of an MPPT algorithm may be offset by the power dissipation of a processor (such as a microcontroller) used to execute the algorithm. Therefore, MPPT is not considered for our TEG.

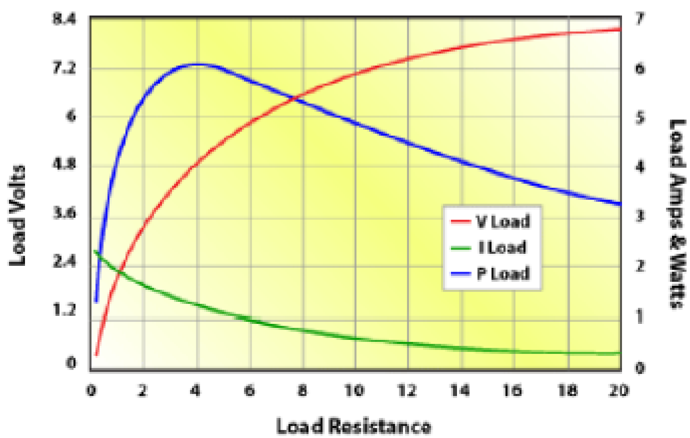

Figure 2.TEG Output Characteristics Error! Reference source not found.**[2]**

2.2 Battery Charging

In order to avoid damaging a battery, voltage and current must be regulated during charging. A multi-stage charging scheme charges a battery more quickly and efficiently. Charging begins with the constant current charging for lithium-ion batteries. Specifically, the rated charge current of the battery is applied, while the battery voltage is monitored. When the voltage reaches a predefined threshold, the charging current is reduced, and the battery voltage is held constant. This stage of charging is commonly called constant voltage charging. The charger remains in this stage until the charging current reduces to a threshold, which is a small percentage of the battery's rated capacity called C-rate. Once this threshold is reached, charging is terminated. The charging process of a lithium-ion battery is illustrated in Figure 3. In the first hour of charge, 1 A of current is injected into the battery. As the voltage reaches above 4 V, the current exponentially decreases as the batteries voltage is held constant. When the charging current drops below 3% of the battery's rated current, charging is terminated. After charging, a small topping current is applied as needed to compensate for self discharge. [1]

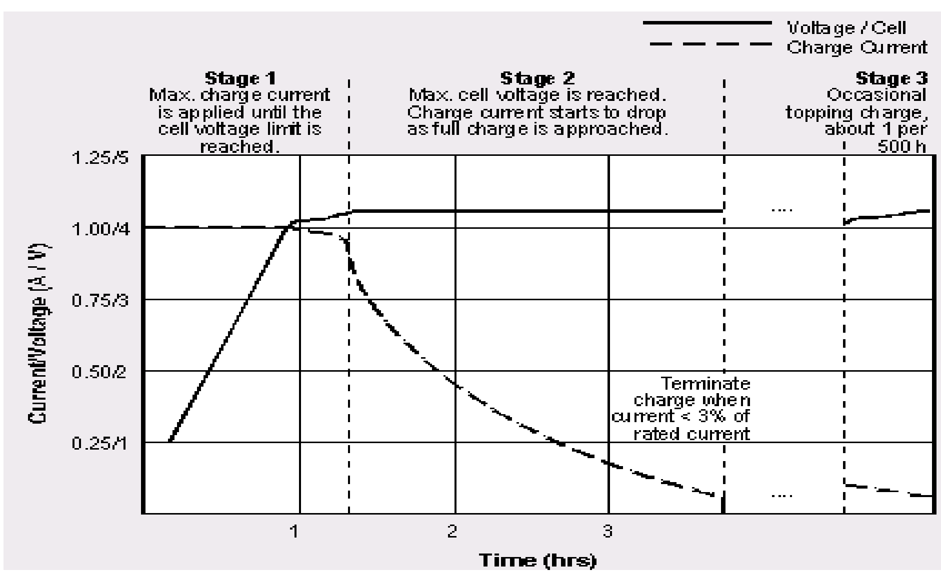

Figure 3.Multi-stage Charging Scheme for Lithium-ion Batteries[1]

If the available charge current is a small fraction of the battery's C-rate, a constant voltage mode may be eliminated without deteriorating the charging performance significantly [1]. In addition, elimination of the mode simplifies the charging circuit to reduce the power consumption of the battery charge circuit. The available charging current is relatively small for our system compared with the battery's C-rate, and constant voltage mode was not used for the system.

2.3 Buck-Boost Converter

A generic buck-boost converter along with some relevant waveforms is shown in Figure 4. Note that the output voltage is inverted in the figure. The transfer characteristics with respect to the duty cycle are dependent on the operating mode of the converter, which is defined by the current flowing through the inductor. If the current flowing through the inductor is always non-zero, the operation is called Continuous Conduction Mode (CCM). In contrast, if the current drops to zero for a portion of the switching cycle, it is called Discontinuous Conduction Mode (DCM). DCM offers simplified system dynamics that improve stability for many control schemes [4]. Poorly designed DCM can suffer from low efficiency in some cases since high ripple currents translate to increased conduction losses. DCM operation has been adopted for our system.

The basic operation of the buck-booster converter is as follows. When the voltage at node V_{SW} is high, the MOSFET is turned on and acts as a short circuit. The input voltage then appears across the inductor and the inductor current ramps up as shown in Figure 4 (b). During the time, the input current and the inductor current are the same. Next, V_{SW} goes low, and the MOSFET turns off and acts as an open circuit. The diode turns on and allows the inductor current to charge the battery. During this period, the output current and the inductor current are the same. The inductor current eventually falls to zero as shown in figure 4, and the process repeats. This indicates that the converter is operating in the DCM.

The ability to adjust the input impedance of a converter is important for maximum power transfer. The input impedance of the buck-booster in the DCM operation is expressed as below [5].

$$R_{in} = \frac{2L}{D^2 T} \tag{1}$$

Where, L is the inductance, T the switching period, and D the duty cycle. The input power to the converter is obtained in (2).

$$P_{in} = \frac{1}{2} L I_{PK}^2 F_s \tag{2}$$

Where, I_{PK} is the inductance and F_s is the switching frequency.

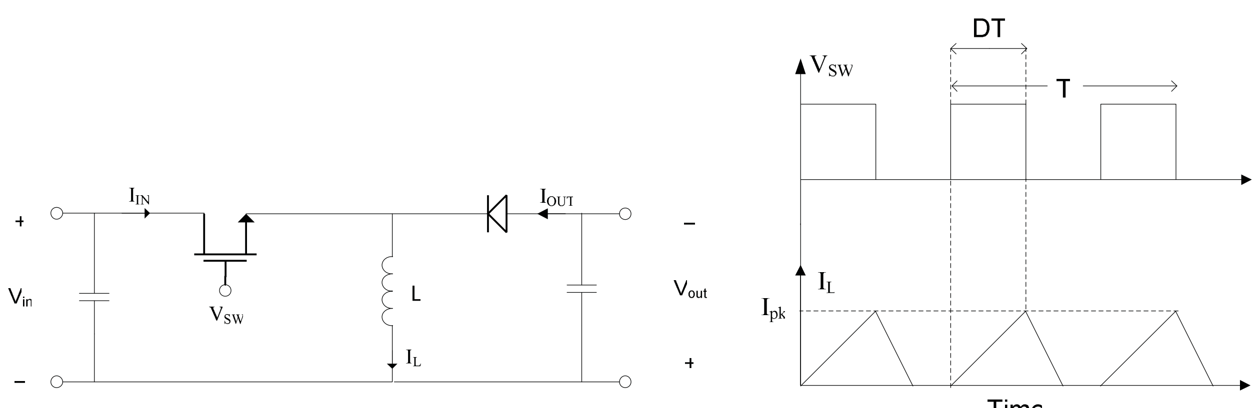

(a) Test circuit (b) Waveform

Figure 4. Buck-Boost Converter and Its Waveforms

3. PROPOSED SYSTEM DESIGN

The proposed energy harvesting system is presented in this section. The overview of the system is described, and then the system design and a buck-boost converter for the solar panel.

3.1 System Overview

Figure 5 shows an overview of the system. The SCANS^n system consumes 8 W of power in active and 100 mW in standby. The energy consumed for the system is about 4.88 W-hours within a 24-hour period. To meet the power and size requirements, a 5 W solar panel (BSP-512 from Powerup) and four TEG devices (28711-5L31-03CY thermoelectric cooling module from Custom Thermoelectric) are selected. The operating voltage of the solar panel is approximately 17 V. Additional power of 100 mW is supplied by a series of four TEG devices with an output voltage of 2 V. MPPT is employed only for the solar panel. MPPT is not considered for the TEG, since the power generated by the TEG is typically too small to benefit from MPPT, and our experiment shows that the optimal resistance stays approximately the same for the range of temperature gradients of our interest. As a result, a fixed duty cycle is supplied to the TEG converter. A 14.4 V, 69 W-hour lithium-ion battery is selected for our system due to its high energy density, high output current capability, and low self-discharge. The battery includes an internal temperature sensor to terminate charging when the temperature reaches a critical value, which prevents thermal runaway.

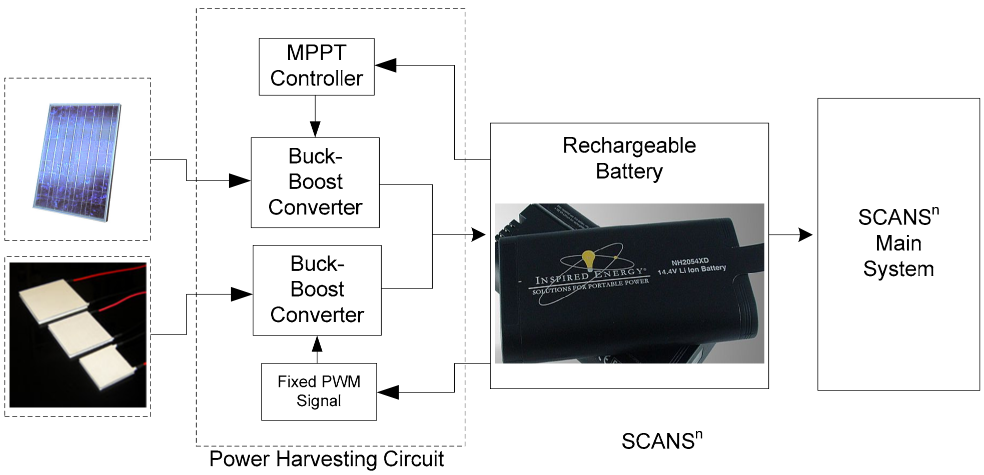

Figure 5. Proposed Energy Harvesting System

3.2 Design of the System and Circuit

Figure 6 shows a Fresnel dome, in which four TEG devices are placed inside the dome. Heat from solar energy is concentrated inside the dome. The hot side of the TEG devices faces the inside of the dome, while the cool side rests against a heat sink that is cooled by the outside environment. The Fresnel dome is realized with a solar lighting dome from Solatube.

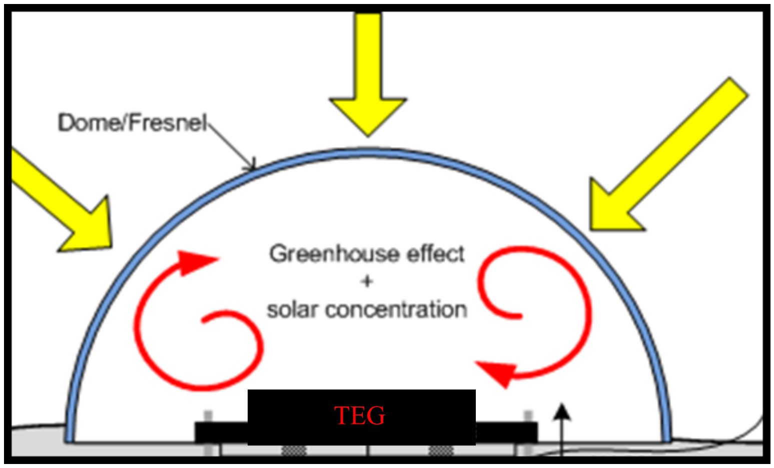

Figure 6. Fresnel Dome for the TEG

Two buck-boost converters operate in parallel to process power harvested from the solar panel and TEGs. As mentioned in Section 2, the input resistance of a buck-boost converter in the DCM mode is a simple function of the duty cycle, which simplifies implementation of the MPPT algorithm. A buck-boost is able to deliver power for a wide range of the input voltage, which is important for the solar panel. Note that the output voltage of the solar panel can vary above and below the battery voltage.

A simplified schematic of the buck-boost converter for the solar panel is shown in Figure 6. A differential amplifier U4 monitors the inductor current through the voltage drop of a small shunt resistor R_{SH}. It should be noted that the current could be monitored at the source of the MOSFET M1, but large transients caused by the large gate-source signal distort the resulting waveform. A scaled down battery voltage V_F and the inductor current I_L are input to a low-power microcontroller MSP430 (U2), which performs MPPT based on the voltage V_F and the current I_L. Voltage V_F is also used to determine when to stop the charging. The pulse width modulation (PWM) signal generated by the microcontroller is boosted by a MOSFET driver U3, which provides an on-voltage V_{BAT} and an off-voltage of approximately 0 V to switch the MOSFET.

A linear regulator U1 generates regulated voltage of 3.3 V, which provides supply voltage for the differential amplifier U4 and the microcontroller U2. The two capacitors C_{in} and C_{out} filter out high frequency switching noise at the input and output of the converter, respectively.

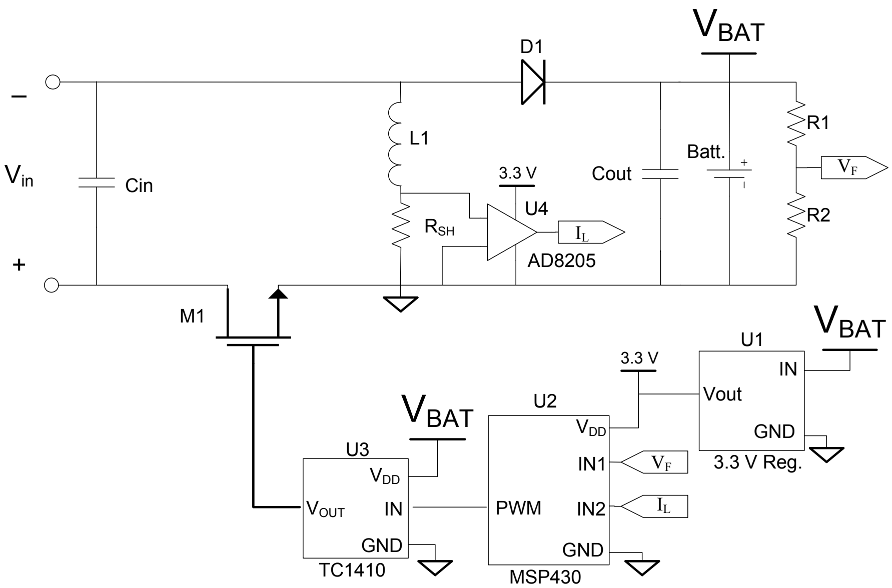

Figure 6. Buck-boost Converter for the Solar Panel

As noted earlier, the buck-booster for the TEG system does not employ MPPT. It implements a fixed duty cycle, using the same MSP430 to generate a PWM, which is capable of driving a low turn-on NMOS without a driver. The MSP430 uses a hardware timer to generate the PWM, so that the only computational power used by the addition of the second PWM is approximately 5 commands on startup. Operating the TEG PWM from the microprocessor did not produce a measureable difference in the power consumed by the MSP430. Thus, the only active component used in the TEG circuitry which is not shared by the solar circuit is the single NMOS in the buck-boost converter. Because the TEG control circuitry only drives the gate of this NMOS, there is essentially no power dissipated by the control for the TEG circuit. The result is that during parallel operation the only losses associated with the TEG are conversion losses, so that while the solar power is operational the battery does not have to invest any additional energy to harvest the thermal energy. This allows the harvester to have an alternate source of power without additional control circuitry.

The C-rate of the selected battery is much higher than the combined output power of the solar panel and the TEGs. Our system simply provides the maximum possible charging current to the battery. When the appropriate floating voltage is reached for the battery, the control circuitry terminates the charging. Due to the thermal runaway with lithium-ion batteries, the temperature is monitored via a thermistor built into the battery. The charge is terminated if the temperature of the battery exceeds the rated one. Note that this circuitry is omitted in Figure 6.

3.3 Impedance Matching for TEG

Because the TEG buck boost would be modulated by a constant PWM, the characteristics of the PWM must be chosen for good power transfer under various conditions. To accomplish this, experimental data was gathered on two different temperature gradients. The gradients were not chosen for emulation of realistic outdoor conditions, but instead exaggerated to see change in the curve as the average temperature changes. Figure 7 shows curves for two temperature gradients with an offset of average temperatures.

The data in Figure 7 supports our decision to avoid MPPT for the TEG power harvesting circuit. Because of the low output power, and the relatively constant output between 50 Ω and 100 Ω, MPPT would not be able to justify the power investment required for tracking. Between the values of 50 Ω and 100 Ω on both curves about 5mW of difference in power was seen, and creation of an effective current sense scheme which loses less than 5 mW would be challenging, and provide little return. Based on this data, the inductance and Equation (1), a duty cycle of 30 % with a frequency of 25 kHz was chosen, to produce an effective input resistance of 55 Ω.

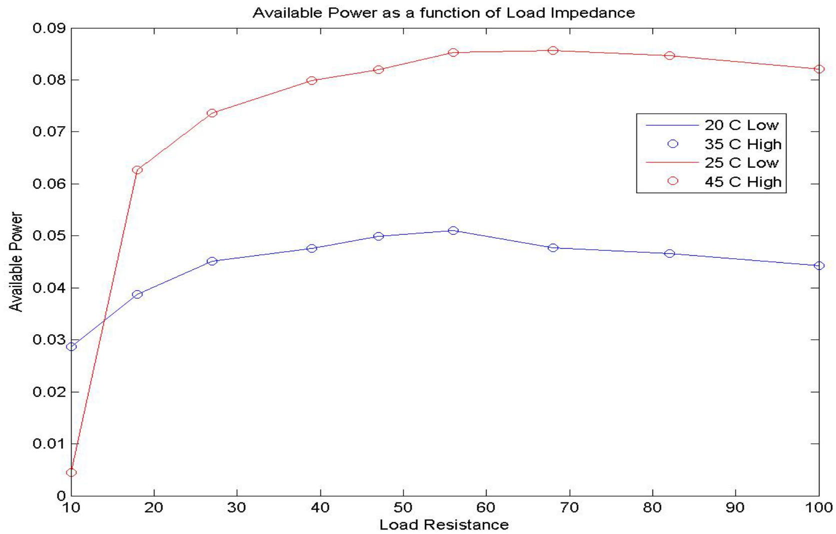

Figure 7. Temperature curves for 20C, 35C and 25C, 45C Cold and Hot temperatures respectively

3.4 Maximum Power Point Tracking for Solar

The microcontroller implements an MPPT algorithm for the solar panel. A hill-climbing or "perturb and observe" algorithm was used, which operates as follows [6]. The duty cycle is initialized to a predefined value. A series of inductor current samples are taken just before the peak current, and the average power is calculated using (2). Note that sampling at the peak current time (right after the MOSFET turns off) results in a large error due to the transition of the current from the MOSFET to the diode. The calculated power is stored, and the duty cycle is incremented in a predetermined step size. Then another series of inductor current samples are taken, and the new power is calculated. If the new power is greater than the previous one, the decision to increase the duty cycle is correct, and the duty cycle is incremented again if not, the duty cycle is decremented back to the more effective value. As the process repeats, the controller will change the duty cycle to reach the maximum power point. When the circuit reaches the MPP, the microcontroller will go into Low Power Mode for approximately 10 seconds to reduce power consumed by control circuitry. Figure 8 (a) shows the test circuit, and Figures 8 (b) and (c) plot the input power from the solar panel and the duty cycle, respectively (to illustrate continued operation of the algorithm, the pause at a MPP is not shown). Initially, both the duty cycle and the power are low. As the duty cycle increases, so does the power. Once the input power reaches 5 W, the duty cycle bounces around the maximum power point.

The hill-climbing algorithm is known to be vulnerable rapid transitions involving increased power occurring over a time on the order of ten iterations of the algorithm. An input such as this can cause the algorithm to continue moving in an incorrect direction for a long period of time, as the observed power delivered to the battery will increase regardless of any relation to the actual maximum power point. Tracking in this case was not attempted, as there are two changing independent variables (load impedance and available power) and only one observed dependent variable (current across inductor). To reduce the effect of rapid transitions, the algorithm had a counter was given a counter and would turn around if it had taken five steps in the same direction, without stepping backwards at least once. The effect of this change is that when rapid transitions occur, the tracker will oscillate around the starting place until the transition settled, and would begin searching after the transition settled. The drawback of this method is that if the algorithm has many steps to move in the same direction, the algorithm may not be able to approach the MPP as fast.

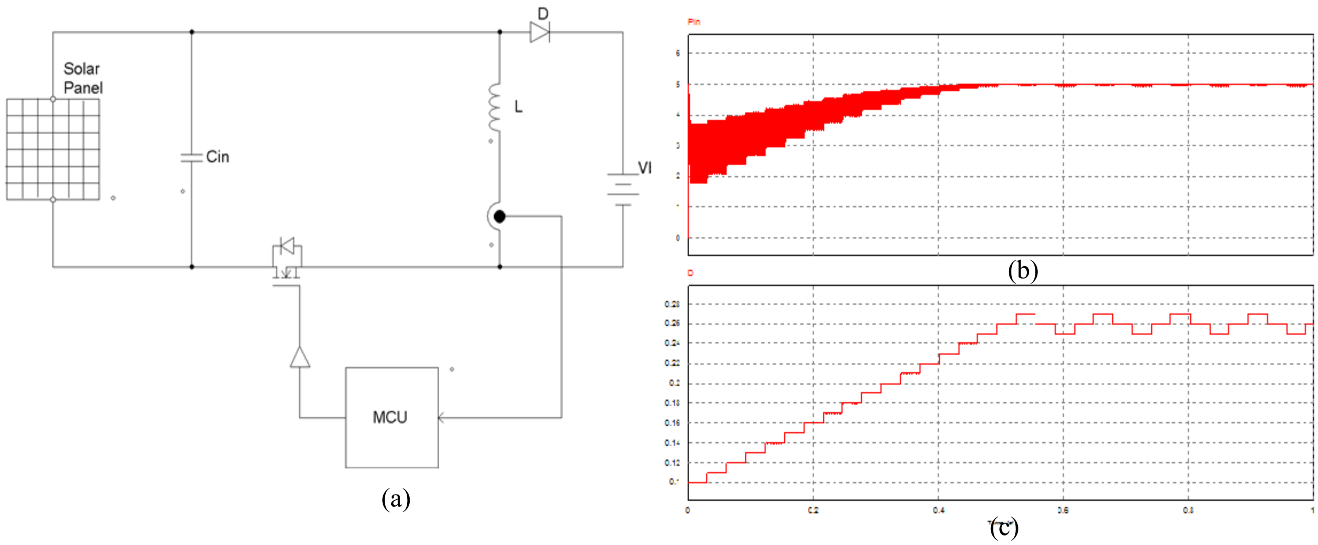

Figure 8. Simulation Result of the Hill-climbing Algorithm

4. EXPERIMENTAL RESULTS

We developed a prototype of the system, and this section provides experimental results of the prototype system.

4.1 Test Setup

The experiment setup for the solar panel is shown in Figure 9. A 400 W Metal-Halide lamp is used to emulate solar irradiance in the lab. The irradiance level is changed by changing the distance between the lamp and the solar panel.

Figure 9.Solar Panel Test Setup

The TEG setup for our prototype is shown in Figure 10. A PID controller controls the hot side temperature of the TEGs, and a heat sink and small fan are used to keep the cool side temperature around 25 °C. A thermocouple is placed between the heat sink and TEGs to measure the cool side temperature. Note that a Fresnel dome is not built for the prototype.

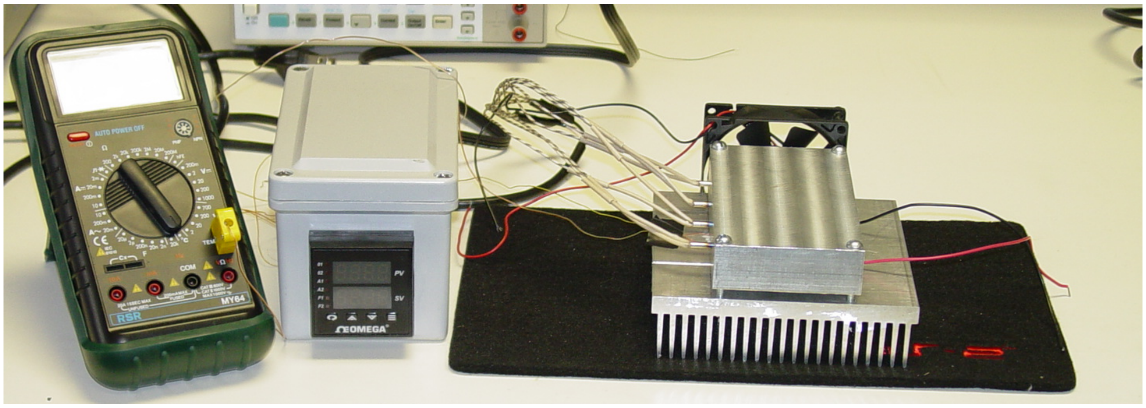

Figure 10.TEG Setup

4.2 Experimental Results

Initially, both the solar and TEG setups were tested separately to understand and optimize each circuit for the real world. A bench top power supply was used to replace the battery as it would allow easier regulation of voltage, and the results would not be dependent on the charge state of the battery. After the circuits were tested separately, the entire circuit was tested together to ensure that operation did not change with both circuits in parallel.

The control circuitry was used to drive the MOSFETS without connecting to the input power, to estimate the power dissipated by the control circuitry. Approximately 4.61 mA at 14.4 V were consumed by the control circuitry, corresponding to about 66.3 mW.

To ensure that the solar circuit MPPT was properly implemented, a characteristic impedance curve was measured using a variable resistor and digital multimeters. Figure 11 shows a characteristic curve for the solar panel with varying load resistance. The curve varies based on the temperature of the panel, which was prone to fluctuate during testing due to the heat from the lamp. In this test the ideal input resistance is in the vicinity of 100 Ω.

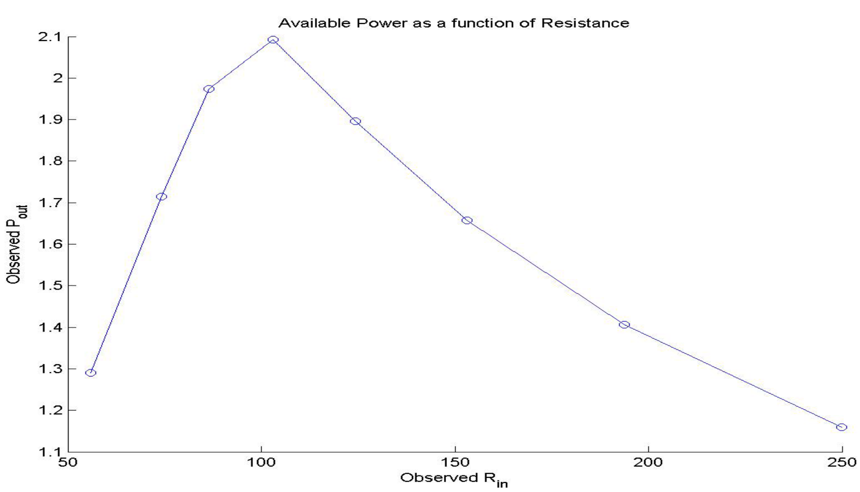

Figure 11. Available power from solar Panel as a function of input resistance

The solar panel was connected to the buck boost converter with the MPPT algorithm and digital multimeters were used to measure currents and voltages coming in and out of the buck-boost converter. As predicted, after an initial transient state, the MPPT algorithm oscillated slightly around a fixed point, under steady state conditions. The center of the oscillations yielded a calculated input resistance of approximately 94 Ω measured input resistance was 101 Ω. 2.52 W were measured available at the output, with 2.09 W delivered to the load. This corresponds to 80.5 % of power being delivered to the battery, with 2.6 % of power dissipated by the control circuitry, and 16.7 % of available power to conduction losses. The MPPT algorithm performed as expected, tracking to the MPP regardless of initial settings.

The thermal system was connected to the buck-boost circuit with constant PWM. The TEG was heated to have a hot side temperature of 44 ^{o}C and a cold side temperature of 30 ^{o}C. Digital multimeters observed 1.711 V and 30.4 mA of power or 52.0 mW available at the input, and 41.9 mW of power delivered to the load. This corresponds to 19.5 % of the power dissipated as conduction losses, a calculated input resistance of 55 Ω and a measured input impedance of 56 Ω.

The two systems were connected in parallel to the power supply. Calculated conduction and control losses remained approximately the same, as did available power. As expected, the current being delivered to the battery was the sum of the current that each individual component was capable of delivering.

Most of the power for the SCANS^{n} system is being provided by the solar panel. To keep the battery breaking even, the solar panel will need to be exposed to lighting conditions similar to that of the lab tests for less than 2.5 hours per day. The presented DC/DC conversion circuit for the TEG adds no new control losses, and delivers more than 80 % of power to the battery but it is still not significantly increasing the rate of charging. Buck Boost converters are known to scale well for larger input voltages and currents, and with minor adjustments, a larger amount of power could be effectively converted. The TEG setup currently takes up approximately 25% as much surface area as the solar setup, and by increasing the size, the TEG could be made to serve as a more viable alternate power source.

Our prototype system successfully demonstrates that SCANS^{n} system can be powered by the energy harvested form solar and thermal.

5. SUMMARY

This paper presents an energy harvest system that could be used to power the SHM system SCANS^{n} developed by Acellent Technologies. The power harvesting system harvests energy from both solar and thermal sources to recharge the lithium-ion battery of SCANS^{n}. During shading of the solar panel, the TEG continues to supply power to the battery charger. Since the output voltages and currents of the solar and thermal energy harvesters vary significantly, the energy harvesting system is constructed by two buck-boost converters operating in parallel. MPPT is employed for the buck-boost converter for the solar panel, while a fixed duty cycle converter is used for the TEG due to substantially lower power compared with the solar panel. The system design and measured results of a prototype were presented. Our prototype system successfully demonstrates that SCANS^{n} system can be powered by the energy harvested form solar and thermal.

REFERENCES

[1] "Low Power Energy Harvesting -- Making the Difference with Efficient Power Management," Special Presentations in IEEE the Applied Power Electronics Conference and Exposition (APEC), Washington DC, USA, Feb, 2009.

[2] Tellurex, "Thermoelectric Module Specifications," G1-1.4 -219-1.14 datasheet, www.tellurex.com/pdf/G1-1.4-219-1.14.pdf

[3] *Charging Lithium-Ion Batteries*, Available in Http://Batteryuniversity.Com/Learn/Article/Charging_Lithium_Ion_Batteries [Feb. 26, 2011].

[4] R. W. Erickson and D. Maksimovic, *Fundamentals Of Power Electronics*. Norwell, Mass.: Kluwer Academic, 2001.

[5] N. Kong, T. Cochran, D.S. Ha, H.-C. Lin, D.J. Inman, "A Self-powered Power Management Circuit for Energy Harvested by a Piezoelectric Cantilever," Applied Power Electronics Conference and Exposition, pp. 2154 -2160, February 2010.

[6] T. Esram and P. L. Chapman, "Comparison of Photovoltaic Array Maximum Power Point Tracking Techniques," IEEE Transactions on Energy Conversion, Vol. 22, pp. 439-449, July 2007.